

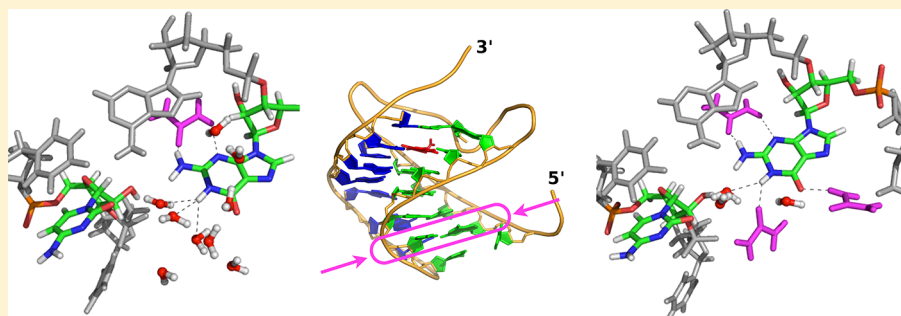
Urea-Induced Denaturation of PreQ₁-Riboswitch

Jeseong Yoon,[†] D. Thirumalai,[‡] and Changbong Hyeon^{*,†}

[†]School of Computational Sciences, Korea Institute for Advanced Study, Seoul 130-722, Korea, and

[‡]Institute for Physical Sciences and Technology, University of Maryland, College Park, Maryland 20742, United States

S Supporting Information



ABSTRACT: Urea, a polar molecule with a large dipole moment, not only destabilizes folded RNA structures but can also enhance the folding rates of large ribozymes. Unlike the mechanism of urea-induced unfolding of proteins, which is well understood, the action of urea on RNA has barely been explored. We performed extensive all-atom molecular dynamics simulations to determine the molecular underpinnings of urea-induced RNA denaturation. Urea displays its denaturing power in both secondary and tertiary motifs of the riboswitch structure. Our simulations reveal that the denaturation of RNA structures is mainly driven by the hydrogen-bonding and stacking interactions of urea with the bases. Through detailed studies of the simulation trajectories, we found that geminate pairs between urea and bases due to hydrogen bonds and stacks persist only ~ 0.1 – 1 ns, which suggests that the urea–base interaction is highly dynamic. Most importantly, the early stage of base-pair disruption is triggered by penetration of water molecules into the hydrophobic domain between the RNA bases. The infiltration of water into the narrow space between base pairs is critical in increasing the accessibility of urea to transiently disrupted bases, thus allowing urea to displace inter-base hydrogen bonds. This mechanism—water-induced disruption of base pairs resulting in the formation of a “wet” destabilized RNA followed by solvation by urea—is the exact opposite of the two-stage denaturation of proteins by urea. In the latter case, initial urea penetration creates a dry globule, which is subsequently solvated by water, leading to global protein unfolding. Our work shows that the ability to interact with both water and polar or nonpolar components of nucleotides makes urea a powerful chemical denaturant for nucleic acids.

■ INTRODUCTION

Neutral in charge, but with a large dipole moment (4.56 D) and a size comparable to water, urea is a versatile chemical agent that can interact with both polar and nonpolar components of biopolymers.¹ Because of its ability to denature folded states, urea has long been used to study the thermodynamic stability of proteins and more recently RNA, allowing researchers to infer the kinetic mechanisms of their folding from urea-dependent folding and unfolding rates.^{2,3} Recent experimental studies using hydrogen exchange⁴ and mid-infrared pump–probe spectroscopy probing the orientational mobility of water molecule⁵ have provided additional insights into the molecular mechanisms of how urea destabilizes proteins. In addition, molecular simulations have played a critical role in elucidating the microscopic mechanism of urea-induced denaturation.^{6–12} Given the complexity of water dynamics that is critical in determining the effective forces between solutes in condensed media,¹³ it is remarkable that the hydrogen-bond network of aqueous water is relatively unperturbed by urea even at high

concentrations (Figure S1). This unique property of urea rules out the “indirect interaction model” as a plausible mechanism for the urea-induced denaturation.^{5,9,11} Although the details of the energetics associated with urea–protein interactions are still under active debate, molecular dynamics (MD) simulations have unambiguously shown that urea molecules act thermodynamically like a “surfactant”: first, water molecules in the first solvation shell (FSS) are expelled by making polar interactions (hydrogen bonds) with the surface-exposed amide backbone, and later they intrude into the protein core by interacting with nonpolar hydrophobic and polar side chains.¹¹

More recently, there has been considerable interest in understanding how urea and naturally occurring osmolytes (TMAO, betaine, etc.) affect the conformations of RNA.^{14,15} It is natural to expect that just like proteins, whose folded and unfolded population can be manipulated by cosolvents as well

Received: June 15, 2013

Published: July 17, 2013

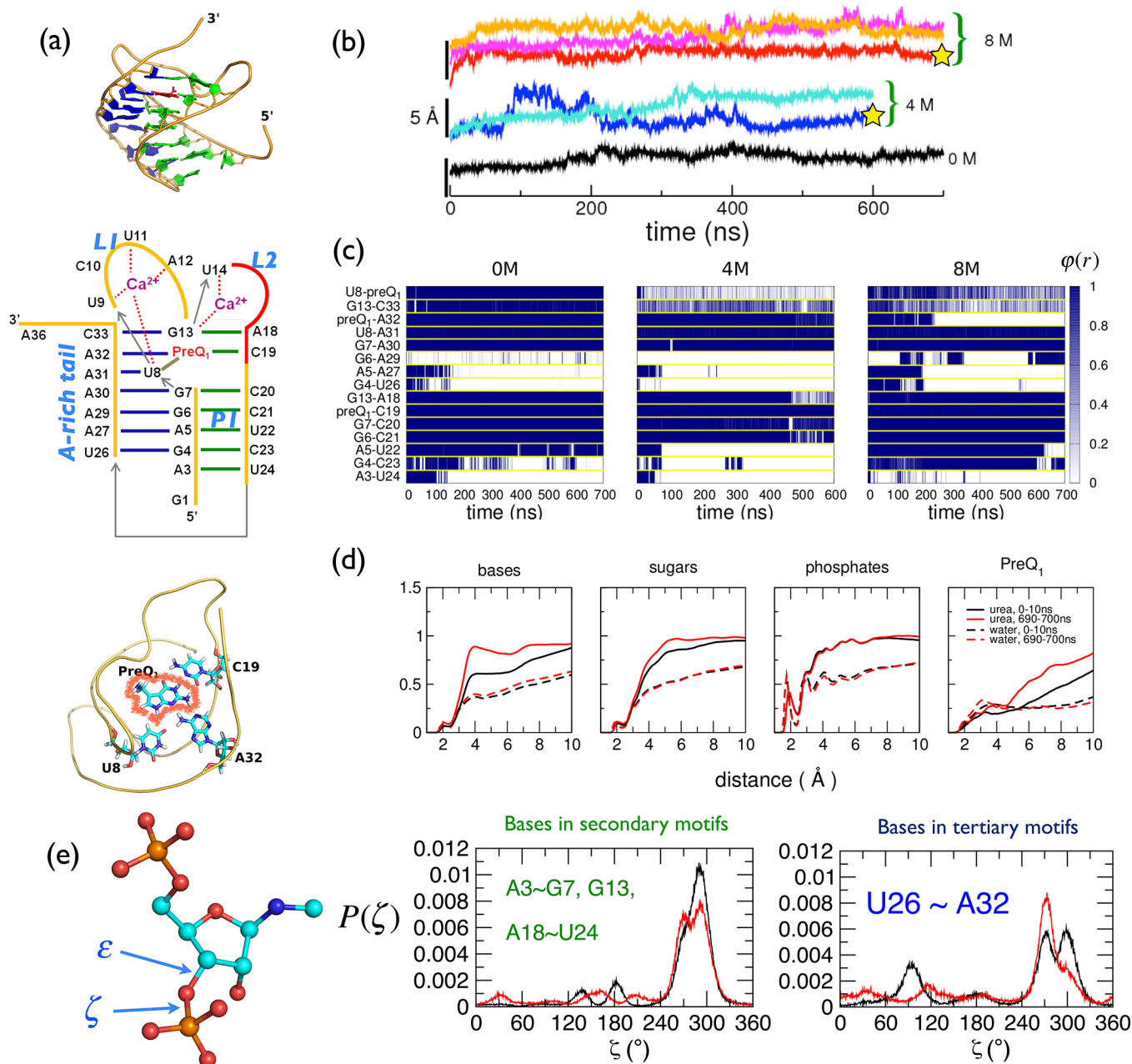


Figure 1. Effect of urea on riboswitch structure. (a) Structure of preQ₁-RS. Diagram below shows base pairs in the RS, with green lines for secondary and blue lines for tertiary interactions. The metastable preQ₁ lies at the center of RS structure, mediating both secondary and tertiary interaction. (b) Time evolution of RMSD of RS. (c) Time evolutions of base-pair contacts at 0, 4, and 8 M urea concentration. The evolutions of contacts for 4 and 8 M were calculated using the trajectories marked with stars in (b). We used $\varphi(r)$, defined in eq 1 in the main text, to visualize the state of each base-pair contact. The scale for $\varphi(r)$ is on the right. (d) Radial distribution functions of water (dashed line) and urea (solid line) around RNA base, sugar, and phosphate of RS and preQ₁ calculated at early (0–10 ns) and late stages (690–700 ns) using 8 M urea trajectory (the rightmost panel in (c)). Here, the distance r is the minimum distance from urea (or water) to any heavy atom in the specified group (base, sugar, phosphate, preQ₁). (e) Distributions of angle ζ for the bases in secondary and tertiary motifs calculated for the first (black) and last (red) 10-ns simulations in 8 M urea.

as temperature, mechanical force, and pressure, RNAs also adapt to changing cosolvent environment.¹⁴ Indeed, with the demonstration that a modest amount of urea can promote folding of misfolded, kinetically trapped structures of *Tetrahymena* ribozyme, urea has also been used as a reagent to probe RNA folding.^{16–19} However, unlike the relatively well understood action of urea on proteins, the detailed molecular mechanism of urea-induced denaturation of nucleic acids has not been explored. Because of the differences in the basic building block between RNA and proteins,²⁰ it is unclear if the

urea-induced denaturation mechanisms of proteins and RNA should be similar. The physicochemical property of the phosphodiester backbone of RNA differs fundamentally from that of a polypeptide chain of proteins. Although the presence of seven torsion angles along the phosphodiester backbone leads to a diversity of the RNA configurations,^{21,22} the RNA backbone itself does not actively participate in stabilizing the RNA structure. The stability of RNA mainly arises from inter-base (base-pairing as well as stacking) and tertiary interactions. These considerations and the ease with which RNA can adopt

alternative structures raise the possibility that interaction of urea on RNA with a tertiary fold can be far more complex than that found in proteins.

Previously we established, using all-atom MD simulation, that urea disrupts RNA base-pair interactions by forming multiple hydrogen-bonding and stacking interactions, thus potentially serving as a surrogate for a base.²³ However, our work was restricted to urea's effects on RNA secondary structures. Here we study the dynamic aspects of how urea disrupts tertiary and secondary interactions in RNA using a 36-nucleotide (nt) *Bacillus subtilis* preQ₁-riboswitch (RS) aptamer domain as a model system. Despite its relatively small size, preQ₁-RS, containing both secondary and tertiary motifs arranged in a characteristic H-type pseudoknot structure,²⁴ is an excellent system for probing the mechanism of urea-induced RNA denaturation from multiple angles. We generated multiple 600–700 ns MD simulation trajectories of preQ₁-RS at three urea concentrations (0, 4, and 8 M) (see Figures 1b,c and S2). Analyses of the trajectories from our all-atom MD simulations have allowed us to discern the microscopic mechanism of urea-induced denaturation and accompanying role of water dynamics. First, as in the earlier study,²³ but here based on a much longer simulation time scale, we show that the major changes in urea and water density occur around nucleobases, which is revealed by visualization of urea and water at early and late stages of the simulation. Second, we study how urea interactions with bases destabilize the secondary and tertiary motifs in the RS structure. Third, we study the kinetics and energetics of urea–base stacking and hydrogen-bonding interactions in detail. Our analyses show that, compared to the time scale of global denaturation process, the lifetimes of urea forming base stacks and hydrogen bonds are relatively short, $\lesssim O(1)$ ns, which indicates that the denaturation of RNA molecule is a consequence of an accumulation of numerous attempts to disrupt intramolecular base–base interactions. These highly dynamic interactions between urea, water, and nucleic acids are exploited to disrupt the inter-base hydrogen bonds and stacks and to stabilize the isolated nucleobases. From a kinetic perspective, we find that in the early stages there is an increase of water population around the bases before the urea molecules start interacting with nucleobase. In other words, the bases are initially destabilized by penetration of water molecules, creating a destabilized “wet” RNA. Only subsequently does urea solvate the solvent-exposed bases. This finding underscores the critical role of water at the early stage of base-pair disruption. The findings from this study, which shed light on the microscopic dynamics of urea and water in the process of RNA denaturation, are amenable to experimental scrutiny.

RESULTS AND DISCUSSIONS

Effect of Urea on the RS Structure. A cognate metabolite, preQ₁, bound to the ligand binding site of preQ₁-RS, consolidates the RS into a characteristic H-type pseudoknot structure, the core part of which is stabilized by the tertiary zipper contacts between the P1 helix (G1-G7, C20-U24) and A-rich tail (A25-A32) (see Figure 1a). PreQ₁ ligand bound to the center of the P1 helix acts as a surrogate nucleotide, stabilizing both the secondary and tertiary structures by forming hydrogen bonds or stacks with five neighboring nucleotides: three in-plane interactions with U8, C19, and A32, and two stacks with G7 and G13.

In the absence of urea, most of the base pairs identified in the NMR structure²⁴ remain intact throughout the 700-ns simulation, except the Watson–Crick (WC) G4-C23 base pair located at the end of P1 helix, the disruption of which leads to an increase of the root-mean-square deviation (RMSD) by ~ 2 Å (0 M trajectory in Figure 1b). Addition of urea to solution destabilizes the RS structure. The overall destabilization of the RS structure at 0, 4, and 8 M urea is visualized using time evolutions of RMSD (Figure 1b) and base-pair contacts involving both the secondary and tertiary structures (Figures 1c and S2). To make clear the distinction between the bound and unbound states of base pairs in Figures 1c and S2, we used a logistic function,

$$\varphi(r) = \frac{1}{1 + e^{(r-r_0)/\sigma}} \quad (1)$$

where r is the distance between the nitrogen or oxygen atom and its partner heavy atom participating in the base-pair hydrogen bond. We chose $r_0 = 5.5$ Å and $\sigma = 0.33$ Å by considering the mean and standard deviation of base-pair distances in the intact state. Interestingly, many of preQ₁-nucleobase pairs (preQ₁-A32, preQ₁-C19) remain intact in our simulation trajectories lasting ~ 700 ns even at 8 M urea (Figures 1c and S2). As a result, we failed to observe the global denaturation of RS structure via disruption of interactions associated with preQ₁. Although 700 ns is clearly not long enough to induce full denaturation of RS (see, however, the Supporting Information (SI) text and Figure S3 for the dynamics of RS upon removal of preQ₁ and Ca²⁺, which shows a larger scale unfolding in the absence of the metabolite and ions), the dynamics of RS structure in aqueous urea displays many interesting features, which shed light on the action of urea on RNA.

Urea and Water Radial Distribution Functions (RDFs) around RS. The change in solution environment around nucleic acid structure reflects the denaturation of RS. RDFs of urea ($g_u(r)$) and water ($g_w(r)$) around base (B), sugar (S), phosphate (P), and preQ₁ (Q)—which we denote as $g_x(r|B)$, $g_x(r|S)$, $g_x(r|P)$, and $g_x(r|Q)$, respectively, with $x = w$ or u , and where the distance r is the minimum distance from urea (or water) to any heavy atom in the specified group—provide a quick glimpse into the solvent structure (Figure 1d; RDFs for other trajectories are in Figure S4). Upon urea-induced destabilization, $g_u(r|B)$ increases with a pronounced peak at 4 Å, indicating that urea molecules make direct interactions with the disrupted bases, while $g_w(r|B)$ shows only a minor increase. The increase of $g_w(r|B)$ is simply a consequence of enhanced exposure of the denatured bases to the solvent environment. The sharp peak of $g_w(r|P)$ at 2 Å (Figure 1d) is due to formation of hydrogen bonds between water hydrogen and phosphate oxygens (see Figure S5). Compared with $g_u(r|B)$, changes in $g_u(r|S,P,Q)$ are all minor, suggesting that a major change in urea distribution upon denaturation occurs around nucleobases, which lends support to our earlier proposal that urea acts as a surrogate base.

Changes in Torsion Angles. The signature of structural destabilization due to urea is reflected in the changes in torsion angles as well. The distributions of seven torsion angles of phosphodiester backbone, calculated for the first and last 10 ns of the trajectories at 8 M urea, reveal that the most distinct changes are in the ζ value defined in terms of O5'–P–O3'–C3' atoms (Figures 1e and S6a). Consistent with our previous study,²³ in aqueous urea solutions the major peak of $P(\zeta)$ at

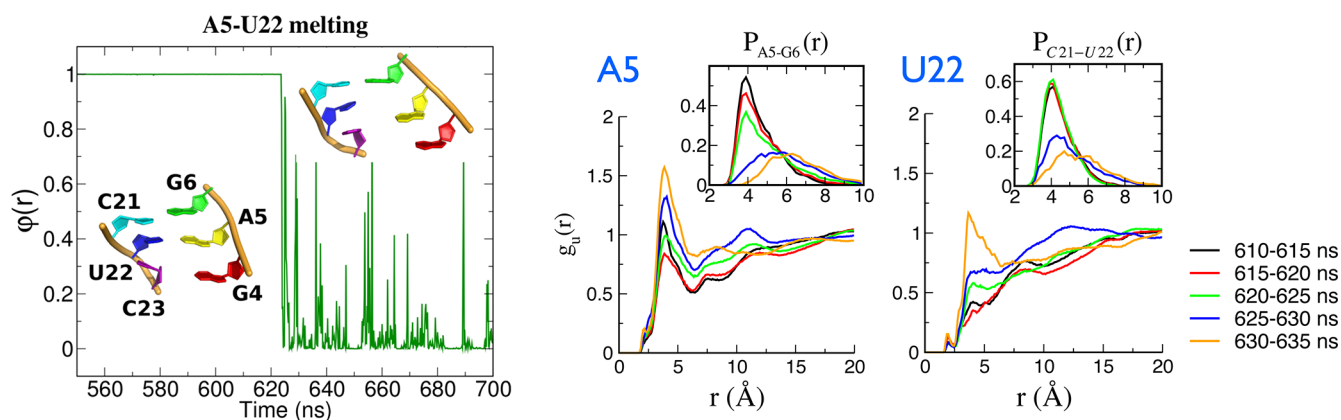


Figure 2. Denaturation of local structures. Destabilization of A5-U22 base pair in 8 M urea quantified using by $\varphi(r)$ (eq 1), and the corresponding changes in RDF of urea during the process of base-pair disruption. Pair distribution functions (insets) show that urea can solvate disrupted bases only when stacking between neighboring bases is removed.

300° shifts to 270° , and a new minor peak at 30° is formed. However, we also found that the $P(\zeta)$ contributed by the tertiary pairs differs greatly from the $P(\zeta)$ associated with the secondary pairs (Figures 1e and S6b). While ζ -values of bases in the stem region are mainly distributed around 300° , G13 and U24 have distinct ζ values because they stack with preQ₁ to form a sharp turn toward U28 via A25. The ζ values for the bases in the A-rich tail vary from base to base and exhibit dramatic changes upon disruption of the base pairs in the sharp turn (U24-U26) and the L1-loop (Figure S6b).

Denaturation of Secondary and Tertiary Motifs of the RS. In aqueous urea, base pairs of RNA exhibit rearrangement as well as disruption. The details of structural changes in RS are determined by the interplay of interactions associated with water and urea, and the degree to which RNA bases are exposed to solvent molecules. Differences in sequence and local environment lead to heterogeneous dynamics of urea-induced destabilization in each base pair.

Removal of Stack from Neighboring Bases Is Critical for Base-Pair Disruption. For a disrupted base to have maximal exposure to the urea environment, the base should be released from the influence of the nonpolar stacking interaction with the neighboring bases. The disruption dynamics of the A5-U22 base pair that lies at the center of the P1 helix, followed by the disruption of the G4-C23 pair, shows this process clearly. The increases in urea population around A5 and U22 occur upon breaking of the A5-U22 base pair, at 620–630 ns (Figure 2). The distribution of A5 relative to the neighboring base G6, quantified by the pair distance distribution ($P_{A5-G6}(r)$), shifts from 4 to 6 Å and broadens with time (see inset in Figure 2), confirming that A5 is released from the stack with G6. A similar pattern of time evolution is seen for U22 in $P_{C21-U22}(r)$ (Figure 2).

Urea Destabilizes Tertiary Structures. Urea-induced dynamics of base pairs in tertiary motifs are considerably more complex than those found in secondary motifs. For example, the non-WC G13-A18 pair, located in the L2 loop with G13 being coordinated to preQ₁, undergoes a more complicated disruption process than the A5-U22 pair (Figure 3a). Examination of the snapshots of structures from simulation (Figure 3a) shows that A18 is fully exposed to the solvent environment while G13 is in complex with preQ₁ even after the G13-A18 interaction is disrupted. As a result, the urea population around G13 remains unchanged, while A18 attracts

urea molecules. There is no significant change in $P_{G13-preQ_1}(r)$ even after the disruption of the G13-A18 pair, which indicates that G13 maintains the stacking interaction with preQ₁.

Base pairs in tertiary motifs are less stable than those in secondary structures. As shown by the RMSD calculated separately for secondary and pseudoknot stacks (Figure 3b), base pairs at the stem region of the secondary structure remain compact, while the tertiary structure, prone to be exposed to the solvent environment, expands readily. The cooperative disruption of Hoogsteen base pairs (G4-U26 and A5-A27) responsible for forming pseudoknot stacks is followed by base-pair rearrangement of G6-A28 to G6-A29. The logistic function $\varphi(r)$ in Figure 3c quantifies how this rearrangement occurred in 600 ns after the base-pair disruption. The $g_u(r)$ (Figure 3c) and $g_w(r)$ (see Figure S7) values summarize the changes in solvent environment around tertiary motifs before and after the denaturations of G4-U26, A5-A27 pairs and G6-A28₁→G6-A29 rearrangement. Both $g_u(r)$ and $g_w(r)$ around G4 and A5 remain unchanged during the denaturation process of G4-U26 and A5-A27 because the base pairs G4-C23 and A5-U22 that stabilize the P1 helix are still intact, making G4 and A5 inaccessible to the solvent (Figure 3c). In contrast, populations of urea and water around U26 and A27 show noticeable increases (Figures 3c and S10).

Similar to G4 and A5, the disruption of Hoogsteen pair G6-A28 does not significantly affect the distributions of urea and water around G6 (Figure 3c) because the WC base-pairing of G6 with C21 in the stem region is still intact (Figure 1). The disruption of G6-A28 increases solvent density around A28 only. In contrast, urea density around A29 decreases due to the formation of a G6-A29 interaction. Taken together, these results show that the degree of urea solvation strongly depends on the degree of inter-base interactions. Most significantly, the stacking interactions between neighboring bases are the key determinant for urea's accessibility and subsequent disruption of the structure.

Stacking and Hydrogen-Bonding Dynamics of Urea with Nucleobases. Although increasing $g_u(r|B)$ suggests that urea stabilizes denatured nucleobases (Figures 2 and 3), the details of the interaction between urea and denatured nucleobase are not well captured by the static $g_u(r|B)$ alone. A careful inspection of the simulation trajectories provides insights into urea configurations that form stacks and hydrogen bonds with bases. In order to visualize the presence of such

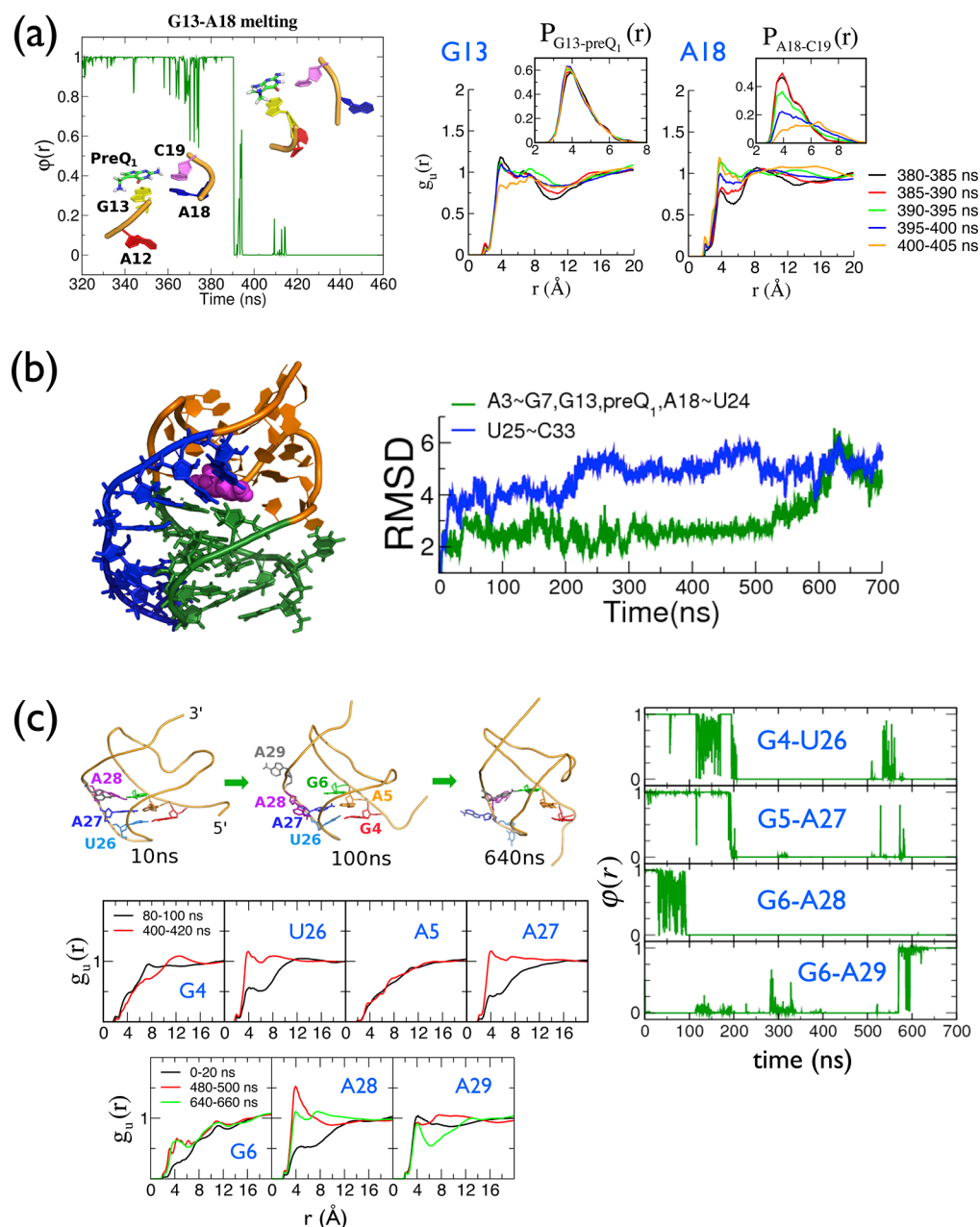


Figure 3. Denaturation of local structures. (a) Dynamics of disruption of the G13-A18 base pair in 8 M urea quantified by the order parameter $\phi(r)$ (eq 1), and the corresponding changes in RDF for urea during the process of base-pair disruption. Pair distribution functions (insets) show that urea can solvate disrupted bases only when stacking between neighboring bases is removed. (b) RMSD of stem+loop region (A3~U24) and tertiary structure region (U25~A33), reflecting the difference in flexibility between the two regions. (c) Disruption and rearrangement of tertiary base pairs of the RS in 8 M urea. Conformational changes of G4, A5, G6 and A26, A27, A28, A29 are illustrated in the snapshots. $\phi(r)$ (eq 1) for each base pair shows cooperative disruption of G4-U26 and A5-A27 base pairs and rearrangement of G6-A28→G6-A29 at 8 M urea. The G6-A28 pair, disrupted at 100 ns, is replaced by G6-A29 at 620 ns. $g_u(r)$ values around each base are shown.

configurations, it is important to define RDFs at the atomistic level. For instance, to identify a configuration of urea stacked on a guanine base, we calculated the RDF between urea carbon (C_u) and the three carbons of guanine base (C2, C4, C5), i.e., $g_{C_u}(r)(C2nC4nC5)_{G4}$, where r is the minimum distance from C_u to any of C2, C4, and C5 in G4 (see Figure 4a). In the case of a hydrogen bond, RDF is straightforwardly defined either between urea oxygen and base hydrogen or between urea hydrogen and base oxygen (or nitrogen) (Figures 4b, S9, and S10b).

The static RDF does not provide the duration of the interactions between base and an individual urea molecule. In solution, more than one urea molecules can interact with a base at a given time. Even if a particular urea–base pair lasts only transiently, exchange with another urea can effectively prolong the lifetime of these interactions. Hence, the distribution of urea around a particular base would be constant if the time scale for averaging were sufficiently long. What is the lifetime of a urea–base interaction? To answer this question, we computed the dwell time distributions for both hydrogen-bonding and stacking interactions (Figures 4 and 5), defined as

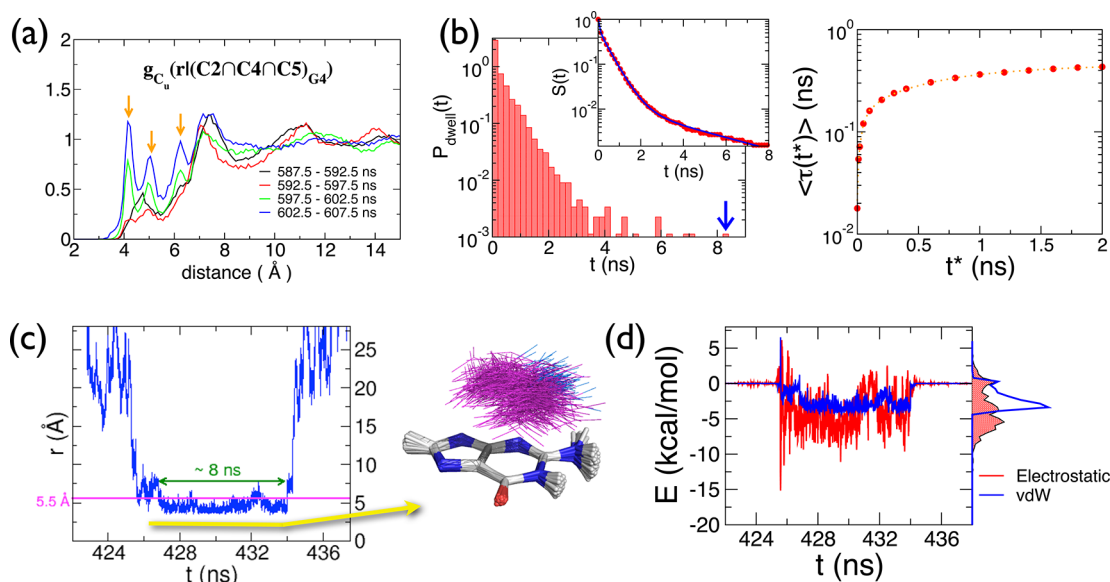


Figure 4. Dynamics of stacking between urea and nucleobase. (a) Development of $g_{Cu}(r)$ between urea carbon and group of carbon atoms in purine ring of G4 during disruption of the G4-C23 base pair. The peaks at 4.2, 5, and 6.3 Å (marked with yellow arrows) reflect formation of stacking and hydrogen-bonding interactions between urea and G4 base as a function of time. (b) Left: Dwell time distribution $P_{dwell}(t)$ and survival probability $S(t)$ for stacking interaction with $t^* = 1$ ns. $S(t)$ can be fit to a triexponential function: $S(t) = \sum_{i=1}^3 \phi_i \exp(-t/\tau_i)$, with $\phi_1 = 0.591$, $\tau_1 = 0.484$ ns, $\phi_2 = 0.395$, $\tau_2 = 0.058$ ns, $\phi_3 = 0.014$, and $\tau_3 = 3.42$ ns, which give the average lifetime of stack $\langle \tau \rangle = \int_0^\infty dt S(t) = 0.365$ ns. One of the longest dwells in the simulation trajectories is $t \approx 8.2$ ns, which is marked with an arrow in $P_{dwell}(t)$. Right: t^* -dependent average lifetime of stack is computed using $\langle \tau(t^*) \rangle = \int_0^\infty dt S(t; t^*)$. The lifetime of the geminate pair of urea–base stack is $\langle \tau(t^* \rightarrow \infty) \rangle = 0.46$ ns. (c) The stack-forming trajectory corresponding to ~ 8 ns dwell time in (b) is shown in the bottom panel. Note that transient disruption ($r > 5.5$ Å) less than $t^* = 1$ ns is still considered as a part of dwell. Structural ensemble of urea molecule stacked on guanine base. Urea oxygen is colored in blue. (d) Stacking energy decomposed into electrostatic and vdW interactions.

$$P_{dwell}(t; t^*) = \frac{1}{N_{dwell}} \sum_{i=1}^{N_{dwell}} \delta[\tau_i(t^*) - t] \quad (2)$$

Because the stacked or hydrogen-bonded configuration, defined on the basis of certain geometrical criteria, is disrupted but reforms transiently, we take the transient disruption time t^* into account in defining the dwell time. This allows us to ignore the transient disruption and reassociation processes whose time lapse is shorter than t^* . In eq 2, $\tau_i(t^*)$ is the time interval of the i th dwell for stacked (or hydrogen-bonded) configuration between urea and base; $\delta[\tau_i(t^*) - t] = 1$ if $t < \tau_i(t^*) < t + dt$, where dt is the size of the time window used to calculate the histogram, otherwise $\delta[\tau_i(t^*) - t] = 0$; N_{dwell} is the number of dwells observed over the entire time traces, with the subscript i denoting the index of the i th dwell. Using the dwell time distribution for a given t^* , $P_{dwell}(t; t^*)$, we can also calculate the survival probability as $S(t; t^*) = 1 - \int_0^t P_{dwell}(\tau; t^*) d\tau$. Thus, the average dwell time for a given t^* is calculated using $\langle \tau(t^*) \rangle = \int_0^\infty S(t; t^*) dt$, and the lifetime of a “geminate” pair between urea and base can be calculated by setting $t^* \rightarrow \infty$ (in practice the upper limit corresponds to duration of the simulation). Below we employ these definitions to evaluate the transient ($t^* = 0$) and geminate pair ($t^* \rightarrow \infty$) lifetimes of stacked and hydrogen-bonded urea–base pairs.

Stacking Dynamics and Energetics of Urea with Nucleobase. When G4 is released from its Hoogsteen partner C23 in 8 M urea at $t \approx 600$ ns (see Figures 1c and 6a), the RDF of urea carbon around the C2, C4, and C5 atoms of G4, i.e., $g_{Cu}(r)(C2 \cap C4 \cap C5)_{G4}$ (Figure 4a), develops three peaks, which reflects the configurations of urea that hovers above the G4 base ring. To analyze the dwell time kinetics of urea–base stacking from time trajectories, we set a distance criterion

for urea–base stack: $\max\{r_{C_u-C2_{G4}}, r_{C_u-C4_{G4}}, r_{C_u-C5_{G4}}\} < 5.5$ Å. The dwell time distribution and survival probability calculated for various t^* values reveal that, although the lifetime of stacking for $t^* = 0$ is less than 0.02 ns, the stack lifetime converges to 0.46 ns when $t^* \rightarrow \infty$ (Figure 4b). $P_{dwell}(t; t^*)$ and $S(t; t^*)$ of stacking interaction for $t^* = 1$ ns are shown on the left panel of Figure 4b. The event marked by the blue arrow in the $P_{dwell}(t)$ is due to the longest dwell event found in a dynamic time trace of urea–base stacking, the actual time trace of which is shown in Figure 4c in terms of urea–base distance as well. The trajectory in Figure 4c shows how a urea molecule approaches the base, maintains stacking interaction for about 8 ns, and subsequently diffuses away (see SI movie 1). The conformation of urea structures that satisfy the above-mentioned distance criterion for stacking lies parallel to the purine ring of a guanine base. It is important to note that the space between the urea–base stack is “dry”, devoid of any water molecule (Figure 4c). Despite the lack of chemical similarity to purine or pyrimidine bases, it is remarkable that urea acts as a base when interacting with guanine.

The non-covalent energy associated with urea–base stacking can be decomposed into electrostatic and van der Waals (vdW) interactions. For the urea stacking on the guanine base, the electrostatic interactions make a greater energetic contribution (~ -5 kcal/mol) than the vdW interactions (~ -3 kcal/mol) (Figure 4d). The larger energetic contribution from electrostatic interaction is due to the attractive interaction between the $O6_{G4}$ and urea hydrogens, and between the urea oxygen and base hydrogens. It is worth emphasizing that the ensemble of urea–guanine stack in Figure 4c displays antiparallel dipole–dipole configurations, in which the urea oxygen faces away from the $O6_{G4}$ to minimize repulsive interactions with $O6_{G4}$ and to

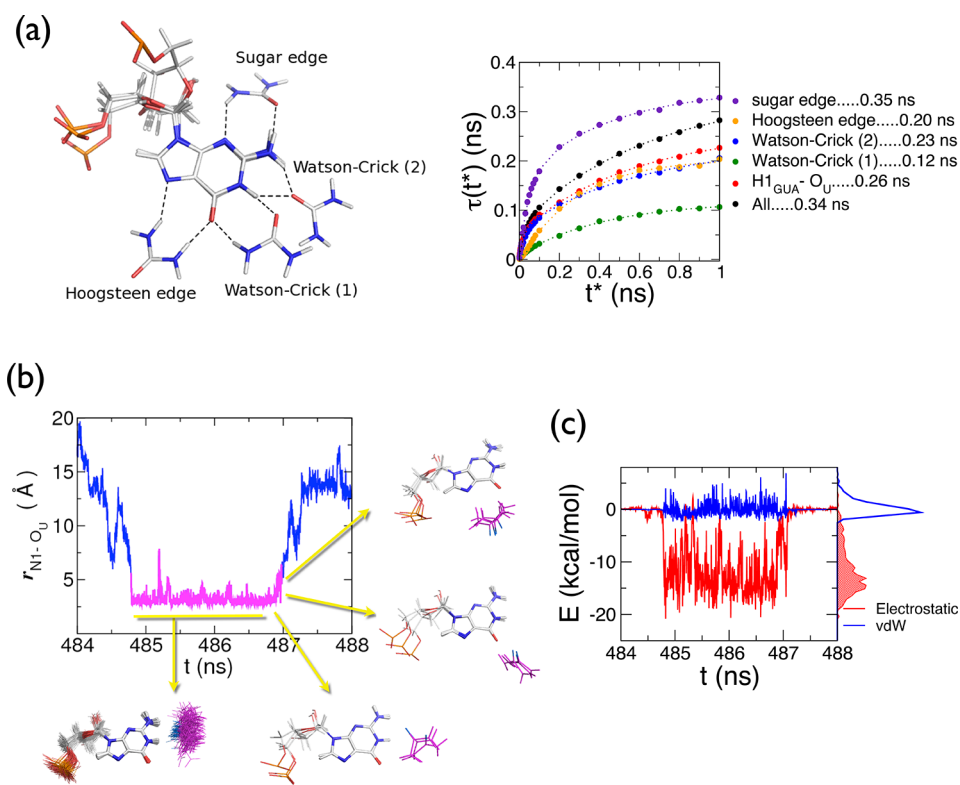


Figure 5. Dynamics of hydrogen-bonding between urea and nucleobase. (a) t^* -dependent average lifetimes of five different types of hydrogen bonds made between urea and base. $\tau(t^* \rightarrow \infty)$ values for different bond types are given in the legend. Configurations of Watson–Crick (1) and (2), Hoogsteen, and sugar edge hydrogen bonds are shown on the right. “All” denotes the union of five types of hydrogen-bonding interactions. (b) The part of the time trace colored in purple corresponds to the time interval in which the urea–guanine hydrogen bond is made. Note that the urea can have various hydrogen-bonded configurations with the base, migrating around the nucleobase while still satisfying the criterion for a hydrogen bond. (c) The energetic contribution of H-bonds decomposed into electrostatic and vdW interactions suggests that electrostatic interaction is the dominant driving force for hydrogen-bond formation.

maximize attractive interactions with hydrogens of N1_{G4} and N2_{G4}. For the urea–adenine stack, the antiparallel dipole–dipole interaction is not as stable as for the urea–guanine stack since the carbonyl group of guanine base is replaced by an amine group in adenine, which renders the electrostatic contribution to the urea–adenine stack essentially zero. However, the urea–adenine stack is stabilized by nearly the same amount of vdW interaction (~ 3.5 kcal/mol) (Figure S8a).

Urea stacking with pyrimidine bases is not as stable as that with purine (guanine, adenine) rings because of the steric hindrance or interaction with phosphate and ribose groups. As shown in SI movie 2, urea spends most of the time interacting with a phosphate group or ribose, which makes urea–cytosine base-stacking incomplete. For uracil, with help from the carbonyl group located at position 4, urea can form a more stable vdW interaction (-2.7 kcal/mol) than cytosine (-1.8 kcal/mol) (Figure S8c and SI movie 3).

Taken together, these results show that stacking interactions of urea with the bases have greater effects on purines than on pyrimidine bases. In addition, it is of note that, although the energetic contribution of the vdW energy due to urea–base stacking is smaller than the electrostatic interactions (Figures 4d and S8), the nonzero value of vdW energy is germane to the urea–base stacks (see below or Figure 5c to compare the vdW energy in urea–base stack with that of urea–base H-bond); thus, one can use vdW energy between urea molecules and

nucleobases to report on the progress of urea-induced denaturation of nucleic acids.

Hydrogen-Bond Dynamics and Associated Energetics of Urea with Nucleobase. Analyses of the trajectories show that there are a few distinct types of hydrogen bonds between urea and nucleobase, which include Watson–Crick, Hoogsteen, and sugar edge hydrogen bonds. We defined the formation of a hydrogen bond by using distance and angle constraints $r_{D-A} < 3.5$ Å, $|\theta_{D-H...A} - 180^\circ| < 45^\circ$, and $|\varphi_{H_U...X1-X2-X3}| < 45^\circ$, where D and A are hydrogen donor and acceptor, respectively, and X1, X2, and X3 are the covalently linked heavy atoms in the base ring, which form a dihedral angle of $\pm 45^\circ$ with urea hydrogen. We relaxed the bond and dihedral angle cutoffs from the usual single hydrogen-bond cutoff value of 30° (ref 25) to 45° because 30° is too stringent to accommodate the geometry of a urea molecule that interacts with a base using multiple hydrogen bonds (see Figure 5a).

Interestingly, bond lifetimes vary greatly depending on the context and type. When t^* is small (less than 5 ps) the lifetime of O_U–H1_G hydrogen bond is the longest, while as $t^* \rightarrow \infty$ the sugar edge hydrogen bond shows the longest lifetime, implying that the former hydrogen bond is energetically more stable while sugar edge hydrogen-bonding holds urea longer. The lifetimes of hydrogen-bondings increase and converge to the values of 0.1–0.4 ns as $t^* \rightarrow \infty$.

Similar to the time trace associated with stacking dynamics in Figure 4c, the time trace of the distance between O_u and N1_G in Figure 5b displays remarkably complex dynamics. The part of

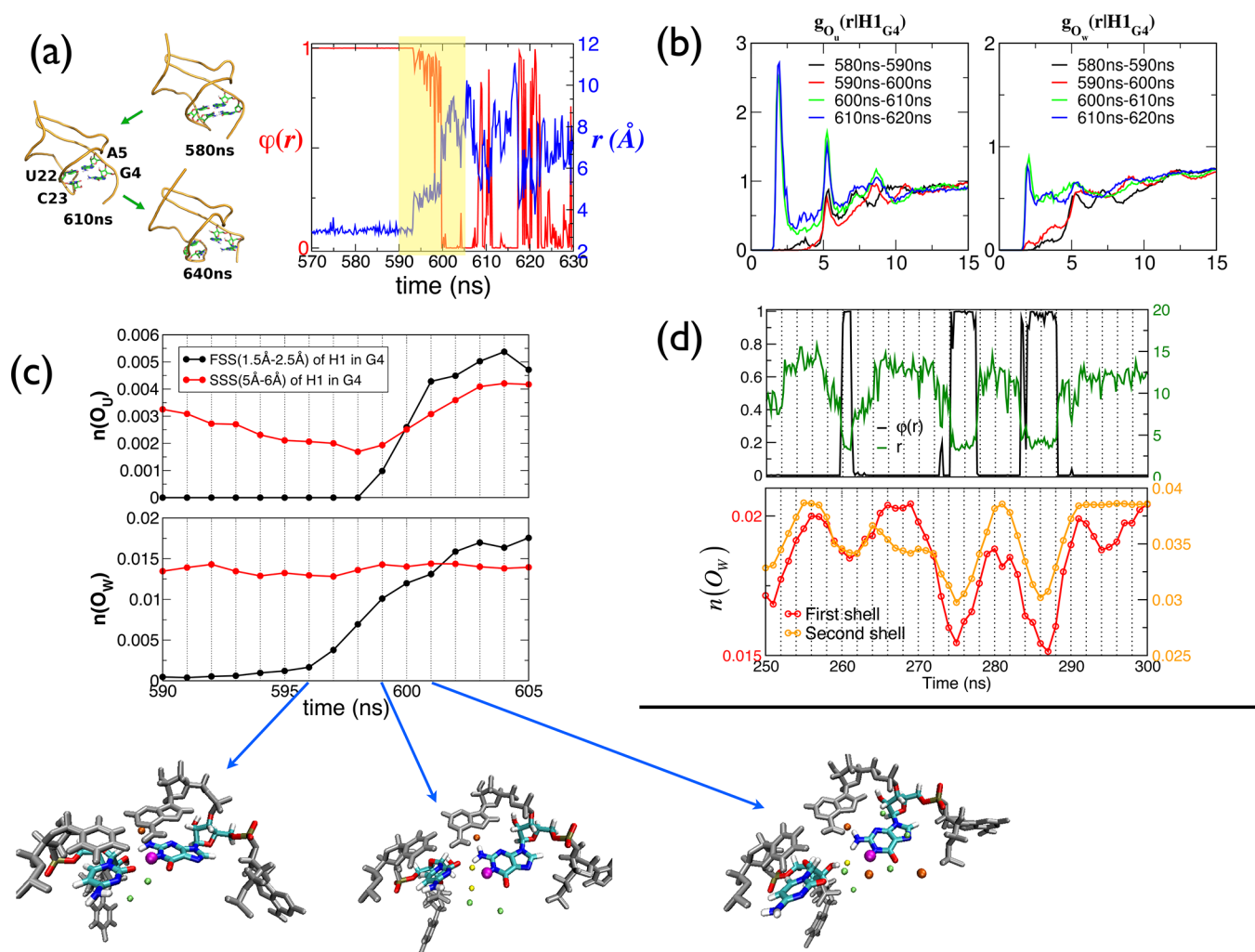


Figure 6. Interplay of dynamics between urea and water molecules in the process of denaturation. (a) Sequential disruption of secondary structure at stem region. The region highlighted in yellow is when G4-C23 base-pair disruption occurs. (b) Change in $g_u(r)$ and $g_w(r)$ around H1 hydrogen atom participating in G4-C23 base-pair interactions. (c) Time evolution of density of oxygens of urea ($n(O_u)$) and water ($n(O_w)$) in the first solvation shell (FSS) and second solvation shell (SSS) of H1 atom of G4 during G4-C23 base-pair disruption. Density of oxygen atoms was calculated using $n(O) = N_{\text{shell}}/V_{\text{shell}}$ where $N_{\text{shell}} = 4\pi\rho \int_{r_{\text{min}}}^{r_{\text{max}}} g(r)r^2 dr$, $V_{\text{shell}} = 4\pi r_c^2 \sigma_{\text{shell}}$, ρ is a bulk density of solvent, $g(r)$ is a radial distribution function, $[r_{\text{min}}, r_{\text{max}}]$ specify the location of a shell, $r_c = (r_{\text{max}} + r_{\text{min}})/2$, and $\sigma_{\text{shell}} = r_{\text{max}} - r_{\text{min}}$. Three snapshots visualize the permeation dynamics of water molecules in the FSS (yellow spheres) and SSS (green spheres), which fill the space between base pairs before a urea oxygen (red sphere) forms a hydrogen bond with $H1_{G4}$ (magenta sphere) (see also SI movie 5). (d) Hydration dynamics for reversible disruption of A3-U24 base pair for urea-free simulation trajectory in the absence of both preQ₁ and Ca²⁺. Shown are the $\varphi(r)$ (eq 1) for $N1_{A3}-N3_{U24}$ distance and time-dependent $n(O_w)$ in FSS and SSS. $n(O_w)$ and $\varphi(r)$ are anticorrelated, which implies that disruption of the base-pair interaction is water mediated.

the trace colored in magenta corresponds to the instance at which the urea–guanine hydrogen bond is formed. Snapshots in Figure 5b show that urea migrates around the guanine base by forming different types of hydrogen bonds. At $t \approx 485$ ns, O_u mainly forms hydrogen bonds with hydrogen atoms in N1 and N2 of guanine. At $t \approx 487$ ns, O_u migrates to O6 to form an O6–urea hydrogen interaction, followed by a Hoogsteen-type interaction, and finally diffuses away from the nucleobase (see also SI movie 4). When the H-bond between urea and O_u base is decomposed into electrostatic and vdW contributions, it is clear that the dominant energy source of H-bond is electrostatic; the vdW interaction makes practically no contribution (Figure 5c).

Dynamic Role of Water Molecules in the Process of Urea-Induced Denaturation. For urea-induced denaturation to occur, both thermodynamic and kinetic requirements should be met so that urea can form a favorable interaction with the

denatured bases, and the intrusion of urea into the narrow space between base–base pairing should occur. Due to their smaller size compared to urea, water molecules can diffuse more easily into various regions of the nucleobases, while urea cannot easily access the space between the stacked bases. It is worth noting that, in our simulations in 8 M urea, the diffusion coefficient calculated using mean-square displacement of water (2.3×10^{-5} cm²/s) is twice that of urea (10^{-5} cm²/s).

Microstructure of Solvent Environment around Nucleobases. To investigate the solvation process in further detail, we calculated the RDFs of urea and water oxygens around $H1_{G4}$ ($g_u(r|H1_{G4})$, $g_w(r|H1_{G4})$), so that the details of the H-bond disruption associated with the G4-C23 pair (Figure 6) could be easily detected. During the destabilization process of the stem region that occurs from the ends of the stack (disruption of G4-C23 pair, followed by A5-U22) (Figure 6a), two sharp peaks develop in $g_u(r|H1_{G4})$ at 2 and 5 Å. The first peak at 2 Å is due

to the hydrogen bond between urea oxygen and H1 of the guanine base. The second peak at 5 Å that appears in the disrupted purine base, but not in the pyrimidine base (see Figure S9), is in fact contributed by the stack between urea and purine base. This finding is in sharp contrast to the relatively structureless $g_{O_w}(r|H1_{G4})$ (Figure 6b).

Water Permeation Precedes Urea–Base Interactions. A careful inspection of RDFs in Figure 6b provides further insight into the dynamics associated with urea and water. At the early stage of destabilization (590–600 ns), urea density at 3–5 Å near the second solvation shell (SSS) (peak at 5 Å) of $g_{O_u}(r|H1_{G4})$ decreases slightly while water density increases in both the FSS and SSS. An increase of water in the region around the FSS is due to the replacement of inter-base hydrogen bonds by water. When the G4–C23 base pair is fully disrupted (600–620 ns), there is a marked increase in urea population in the FSS and SSS, corresponding to formation of hydrogen-bonding and stacking interactions, respectively. To assess the urea and water dynamics during base-pair disruption quantitatively, we calculate the time evolution of the number density of urea oxygen ($n(O_u)$) and water oxygen ($n(O_w)$) in the FSS and SSS of H1 atom in G4 base (Figure 6c). Note that motions of water, urea, and nucleobase are highly dynamic and undergo substantial fluctuations even in the time interval as short as 1 ns. To see the overall changes in the number density of water and urea, we filtered the fluctuations in data by taking the running average over 5 ns. As is clearly shown in Figure 6c, destabilization of the base pair occurs in the following three steps: (1) In the initial stage (590–598 ns), an increase of $n(O_w)$ in the FSS is accompanied by the decrease of $n(O_u)$ in the SSS, which indicates that water permeates into the FSS by expelling urea away from the SSS. This process breaks the hydrogen bonds between base pairs. It is important to note that at $t \approx 598$ ns, when water is present in the FSS, the density of urea is effectively zero (Figure 6c). (2) In the disruption stage (598–602 ns), the numbers of both urea and water molecules increase drastically in the FSS and SSS. The disrupted bases are stabilized by forming multiple hydrogen bonds and stacks with urea. (3) In the late stage (602–605 ns), the water population in the FSS and SSS stops increasing, but urea increases further to fully solvate the bases. The mechanism of cooperative action between urea and water, revealed in the disruption of secondary structure, also holds in the disruption of tertiary structure (see SI text and Figure S10a). Among the steps (1)–(3), of particular note is the initial infiltration of water molecules into the dry and narrow space between base pairs (step (1)), which is an important prerequisite for urea to interact with nucleobases (see SI movie 5 that visualizes water molecules in the FSS (yellow) and SSS (green) in the time interval of 596–601 ns). Only after destabilization of base-pair interaction by penetration of water can urea solvate the nucleobases.

To verify that base-pair disruption is indeed initiated by water permeation, we additionally examined the hydration dynamics around the A3–U24 base pair from a urea-free simulation in the absence of preQ₁ and Ca²⁺ (Figure 6d). As expected, the fluctuation of base-pair distance is correlated with water densities in the FSS and SSS. It is remarkable that, when the time series of water density around A3 and breathing dynamics of the base pair are compared, the change in water density *always* precedes the change in base-pair distance. The increase in water population begins to slow down only after the disruption of the base pair. Conversely, the water population

stops decreasing after base-pair formation is completed. Thus, it follows that the dynamics of water permeation gives rise to the breathing dynamics of base pairs. Urea can stabilize this transiently unbound base pair by forming stacks or multiple hydrogen bonds, which results in denaturation of the base pair.

CONCLUDING REMARKS

Unlike proteins, base pairs—a major building block of structured nucleic acids—are always deeply buried inside the major and minor grooves of folded RNA molecules; thus, there is no water solvation shell that can directly interact with the nucleobases. Displacement of water in the first solvent shell by urea, which was suggested as an early-stage dynamics for urea-induced protein denaturation,¹¹ cannot account for urea-induced RNA denaturation. In sharp contrast, our simulations highlight the early penetration of water in the narrow space between the base pairs or base stack as a critical kinetic step before urea interacts with the bases. Since the phosphodiester backbone does not particularly attract urea molecules, and urea is too big to fit between the nucleobases, the enhancement of structural fluctuations due to water–base interaction is critical for urea to access and interact with nucleobases. Thermodynamic stabilization of disrupted nucleobases by urea's multiple hydrogen-bonding and stacking interactions follows afterward. On the basis of these findings, we propose that the kinetic sequence of destabilization of folded RNA should follow native state → wet state → unfolded state. Because the lifetime of germinate urea–nucleobase pairs is short ($\lesssim O(1)$ ns) (Figures 4b and 5a) compared with the breathing time of base pairs (~10 ns) (Figure 6d), the sequence of events involving urea around nucleobases is highly dynamic.

The high polarity and size comparable to water are the unique properties of urea which enable urea to have high solubility in water without perturbing the structure of water,²⁶ and to interact with various components of nucleic acids by exploiting the ability to engage in a multitude of hydrogen bonds. Besides urea's hydrogen-bonding with nucleobases, we highlighted the ability of urea to stabilize disrupted nucleobases via stacking interactions. Our study shows that the ability to engage in both stacking and hydrogen-bonding interactions makes urea an effective denaturant of nucleic acids.

METHODS

Riboswitch Model. The *B. subtilis* preQ₁-RS aptamer is the only one whose solution and crystal structures have been determined.²⁴ Although the solution and the crystal structure are nearly identical, there are some differences. The crystal structure has several visible Ca²⁺, especially two Ca²⁺ ions in the L1–P2 turn, while Ca²⁺ is not present in solution structure. First, it has been shown that Ca²⁺ ions stabilize the L2 loop. Second, L2 residues are well-defined in the solution structure while they are not resolved in the crystal structure. In our simulations we included two Ca²⁺ ions in the L1–P2 turn from crystal structure into the solution structure (PDB ID: 2L1V).

Simulation Details. PreQ₁-RS is solvated in a 60 Å × 60 Å × 60 Å box containing 6267 TIP3P water. For 8 M urea simulation, 1052 urea molecules were randomly distributed by replacing water molecules in the box. After a short duration when energy minimization was carried out to remove clashes among urea molecules, 51 Na⁺ and 20 Cl[−] ions, which amount to ~150 mM salt concentration in the bulk, were randomly placed. At the equilibration stage we gradually heated the system from 0 to 310 K using 2 fs time steps, and simulated for an additional 100 ps in the NPT ensemble and an additional 100 ps in the NVT ensemble without constraint to ensure pre-equilibration at 310 K. We further equilibrated the urea–RS system for 10 ns by using the NPT ensemble at 310 K and 1 atm. Theories and experiments^{27–29}

show that counterions play a key role in the folding of RNA. The distribution of monovalent counterions (Na^+) on the surface of RS after equilibration is shown in Figure S12. A high density of negative charge is formed at core regions of RS structure where base-pair interactions are made, which is indicated by the value of electrostatic potential from a solution of nonlinear Poisson–Boltzmann equation. It is worth noting that major populations of counterions, calculated from time trajectories from MD simulations, are in the core regions predicted by the nonlinear Poisson–Boltzmann equation to have high negative electrostatic potential. We performed simulations by using NAMD with CHARMM force field for RS and urea. For the force field of preQ₁, we followed the basic philosophy of CHARMM general force field parametrization strategy.³⁰ For consistency with CHARMM force fields of canonical nucleotides, we applied partial charge from the guanine to pyrimidine ring of preQ₁ except for the -C7-CH₂-NH₂ side chain and two carbon atoms directly connected to the C7 atom. For -C7-CH₂-NH₂ and two connected carbon atoms, we assigned partial charges and dihedral force constants by analogy using parameters from residues of similar structure in CHARMM force field as a first guess and refining the parameters in order to produce dihedral angle distribution similar to that of the preQ₁ in solution structure. For production runs, we performed simulations in various conditions, ranging from pure water to aqueous urea solutions of differing concentrations. We simulated one 0 M urea and three 8 M urea each for 700 ns, two 4 M urea each for 600 ns in the presence of preQ₁ and Ca²⁺, and one 0 M urea for 700 ns and one 8 M urea for 600 ns in the absence of preQ₁ and Ca²⁺. The comprehensive simulations provide fundamental insights into the mechanisms of destabilization of folded RNA.

■ ASSOCIATED CONTENT

● Supporting Information

Dynamics of RS upon removal of preQ₁ and Ca²⁺ ions; permeation of water into tertiary motifs; water, urea dynamics in the process of base pair rearrangement; Figures S1–S12; SI movies 1–5. This material is available free of charge via the Internet at <http://pubs.acs.org>.

■ AUTHOR INFORMATION

Corresponding Author

hyeoncb@kias.re.kr

Notes

The authors declare no competing financial interest.

■ ACKNOWLEDGMENTS

We thank the KIAS Center for Advanced Computation and KISTI Supercomputing Center for providing computing resources including technical support KSC-2011- C1-10. D.T. acknowledges support from the National Science Foundation through grant CHE 09-14033.

■ REFERENCES

- (1) Roseman, M.; Jencks, W. P. *J. Am. Chem. Soc.* **1975**, *97*, 631–640.
- (2) Sánchez, I. E.; Kiefhaber, T. *J. Mol. Biol.* **2003**, *325*, 367–376.
- (3) Shelton, V.; Sosnick, T.; Pan, T. *Biochemistry* **1999**, *38*, 16831–16839.
- (4) Lim, W. K.; Bösgen, J.; Englander, S. W. *Proc. Natl. Acad. Sci. U.S.A.* **2009**, *106*, 2595–2600.
- (5) Rezus, Y. L. A.; Bakker, H. J. *Proc. Natl. Acad. Sci. U.S.A.* **2006**, *103*, 18417–18420.
- (6) Kuharski, R. A.; Rossky, P. J. *J. Am. Chem. Soc.* **1984**, *106*, 5794–5800.
- (7) Cafisch, A.; Karplus, M. *Structure* **1999**, *7*, 477–488.
- (8) Mountain, R. D.; Thirumalai, D. *J. Am. Chem. Soc.* **2003**, *125*, 1950–1957.

- (9) O'Brien, E.; Dima, R.; Brooks, B.; Thirumalai, D. *J. Am. Chem. Soc.* **2007**, *129*, 7346–7353.
- (10) Stumpe, M. C.; Grubmüller, H. *J. Am. Chem. Soc.* **2007**, *129*, 16127–16131.
- (11) Hua, L.; Zhou, R.; Thirumalai, D.; Berne, B. *Proc. Natl. Acad. Sci. U.S.A.* **2008**, *105*, 16928–16933.
- (12) Canchi, D. R.; Paschek, D.; Garcia, A. E. *J. Am. Chem. Soc.* **2010**, *132*, 2338–2344.
- (13) Chandler, D. *Nature* **2005**, *437*, 640–647.
- (14) Lambert, D.; Draper, D. *J. Mol. Biol.* **2007**, *370*, 993–1005.
- (15) Pincus, D.; Hyeon, C.; Thirumalai, D. *J. Am. Chem. Soc.* **2008**, *130*, 7364–7372.
- (16) Pan, J.; Thirumalai, D.; Woodson, S. A. *J. Mol. Biol.* **1997**, *273*, 7–13.
- (17) Pan, J.; Thirumalai, D.; Woodson, S. A. *Proc. Natl. Acad. Sci. U.S.A.* **1999**, *96*, 6149–6154.
- (18) Rook, M. S.; Treiber, D. K.; Williamson, J. R. *J. Mol. Biol.* **1998**, *281*, 609–620.
- (19) Pan, T.; Sosnick, T. R. *Nat. Struct. Biol.* **1997**, *4*, 931–938.
- (20) Thirumalai, D.; Hyeon, C. *Biochemistry* **2005**, *44*, 4957–4970.
- (21) Murray, J. J. W.; Arendall, B., III; Richardson, D. C.; Richardson, J. S. *Proc. Natl. Acad. Sci. U.S.A.* **2003**, *100*, 13904–13909.
- (22) Wadley, L. M.; Keating, K. S.; Duarte, C. M.; Pyle, A. M. *J. Mol. Biol.* **2007**, *372*, 942–957.
- (23) Priyakumar, U.; Hyeon, C.; Thirumalai, D.; MacKerell, A., Jr. *J. Am. Chem. Soc.* **2009**, *131*, 17759–17761.
- (24) Zhang, Q.; Kang, M.; Peterson, R. D.; Feigon, J. *J. Am. Chem. Soc.* **2011**, *133*, 5190–5193.
- (25) Luzar, A.; Chandler, D. *Phys. Rev. Lett.* **1996**, *76*, 928–931.
- (26) Wallqvist, A.; Covell, D. G.; Thirumalai, D. *J. Am. Chem. Soc.* **1998**, *120*, 427–428.
- (27) Thirumalai, D.; Lee, N.; Woodson, S. A.; Klimov, D. K. *Annu. Rev. Phys. Chem.* **2001**, *52*, 751–762.
- (28) Koculi, E.; Hyeon, C.; Thirumalai, D.; Woodson, S. A. *J. Am. Chem. Soc.* **2007**, *129*, 2676–2682.
- (29) Moghaddam, S.; Caliskan, G.; Chauhan, S.; Hyeon, C.; Briber, R.; Thirumalai, D.; Woodson, S. *J. Mol. Biol.* **2009**, *393*, 753–764.
- (30) Foloppe, N.; MacKerell, A., Jr. *J. Comput. Chem.* **2000**, *21*, 86–104.